GLOBAL METABOLOMICS ANALYSIS OF PAKISTANI CITRUS CULTIVARS INFECTED WITH HUANGLONGBING OR CITRUS GREENING

[a,b,c]Khadija Gilani, [c]Asma Ahmed, [c,d]Rehana Badar, [c]Shaista Javaid, [c]Mehmood-ul-Hassan, [a]Shagufta Naz, [e]Sami Ullah

[a] Department of Biotechnology, Lahore College for Women University Lahore, Lahore, Pakistan.
[b] Department of Microbiology and Cell Sciences, University of Florida, Gainesville, FL, 32603, United States of America.
[c] Institute of Molecular Biology and Biotechnology, The University of Lahore, Lahore, Pakistan.
[d] Department of Biological Sciences, Superior University, Lahore, Punjab, Pakistan.
[e] Pakistan Agricultural Research Council, Adaptive Research cum Demonstration Institute (ARDI), Tank, KPK, Pakistan.

A R T I C L E   I N F O

A B S T R A C T

Citrus is a significant leading fruit crop in Pakistan, with the highest export volume of 370 million tons. HLB is a bacterial disease that has been a potential threat to global citrus production with no effective cure to date. To fill the gap of existing knowledge of *C*Las and its pathophysiological modification. The infection of *C*Las in citrus trees depends on the metabolites involved inside its metabolic pathways. This study was used to determine the global metabolites involved in the disease citrus greening. The *C*Las infection in citrus cultivars was detected through qRT-PCR. The Ct value ranged from 36.3 or no Ct value for the healthy samples. Here we report the first metabolic profiling of the vast range of targeted metabolites of ten citrus cultivars of Pakistan via LC-MS analysis. Results have been verified via the Tukey test (Pr>|t|), One-way ANOVA (p≤ 0.05), and MetaboAnalyst 5.0 tools (Volcano plot, PCA, 2D and 3D PLS-DA plots, heat maps, VIP scores plot, Permutation test). A total of 500 statistically verified metabolites were detected in the leaves. Negative ion mode indicated 57% of metabolites, whereas 43% were identified in positive ion mode with good separation. Potential differences among the global metabolites of varying classes included sugars, amino acids, organic acids, phenolic acids, organic acids, carboxylic and nucleic acids, and flavonoids in positive and negative ion modes. There was an approximately 50% chance in negative ions that known metabolites separating healthy and HLB-infected leaf samples. Many untargeted compounds were also detected which were not found in the LC-MS (MZmine freeware) database, indicating the possibility of identifying novel metabolites that could be used as molecular markers for HLB diagnosis and management. This study provides a broad picture of the accumulation of metabolites involved in citrus plants with citrus greening. The metabolomic profile indicated the possible changes at the maturing stage of the disease.

Corresponding Author: Asma Ahmed
Email: asma.ahmeduol@gmail.com

INTRODUCTION

Advancements in biological science techniques with the addition of information technology and systems biology approach are important (Svatos, 2011). Genomics, transcriptomics, lipidomics, proteomics, and metabolomics are emerging "omics" techniques that have now become an essential part of biological science studies. Various biochemical compounds and

metabolites such as amino acids, sugars, oligo-peptides, and fatty acids from biological samples are analyzed through metabolomics (Clark *et al.*, 2008; Patti *et al.*, 2012; Liu *et al.*, 2017). Recently, with the advances in science and technology, metabolite profiling of food commodities is used for the determination of food quality and nutritional values (Brennan *et al.*, 2017; Celis-Morales *et al.*, 2017).

Citrus fruits are the major source of vitamin C, minerals, dietary fibers, carotenoids, flavonoids, and other biologically important metabolites essential for human health (Liu *et al.*, 2012). Unfortunately, several bacterial and fungal diseases are currently threatening the survival of the global citrus industry. HLB is the most devastating bacterial disease caused by phloem sap-restricted bacteria, *Candidatus* Liberibacter (*C*Las), disseminated by phloem sap-piercing insects, Asian Citrus *Psyllid* (ACP). Until now, there are no well-known remedies, treatments, or methods with which cultivars can resist Huanglongbing. Infection not only decline the rate of citrus trees within a few years but also produced inedible fruits that are not suitable for fresh consumption, juice manufacturing, and exportation of citrus fruit due to a substantial upsurge in acidic with bitter off-flavor fruit production (Bove *et al.*, 2002; Munir *et al.*, 2022).

Candidatus Liberibacter is a phloem-limited, fastidious, gram-negative bacterium that causes Huanglongbing. Asian Citrus *Psyllid* (ACP) is the main vector responsible for spreading this disease (Hall *et al.*, 2013). It consists of three species: asiaticus (Ikpechukwu *et al.*, 2012), africanus, and americanus (Martinelli *et al.*, 2017). There are two psyllid vectors responsible for the transmission of the bacteria. *Diaphorina citri* and *Trioza erytreae* (Hilf *et al.*, 2020). In Pakistan *Candidatus* Liberibacter asiaticus has been only detected transmitted through *Diaphorina citri*. The vector lay eggs on the citrus trees using the psyllid, which introduced the bacterium into the phloem sap and allows it to take its food from the vascular system of plants. It has inflicted vast economic losses worldwide attributed to inedible bitter taste fruit with high levels of fruit drop at early stages of development. It is a graft-transmissible disease, which significantly contributes to its spread through grafting (Roistacher, 1991). The symptoms of HLB include blotchy mottling of leaves, twig dieback, and ultimately, drop of fruit from the tree. The *C*Las-infected fruit may be lopsided and remain green at the stylar end, containing aborted bitter-taste seeds and discolored vascular bundles. Most of the time, *C*Las-infected fruit are asymptomatic from healthy fruit (Siddique *et al.*, 2018). The HLB has caused devastating effects on the citrus world industry in Asian and African countries for decades. The economic losses of citrus are due to the long period of dormancy between the bacterial infection and manifestation of this disease and the fact that the symptoms have close similarities to other citrus diseases. Early detection of HLB was detected by using the SEM. However, the significant bacterial titer was confirmed by using PCR techniques. In Pakistan, 198,983 ha of citrus harvested area was used for cultivation. It increased from 43,900 to 198,983 ha from the years 1971 to 2020 with 3.32% of the annual average rate. There was 2.89 million tons production of citrus reported in Pakistan in 2021 (Sajid *et al.*, 2022).

Plant metabolomics is an important tool for understanding the metabolism of several plant diseases. It is used to measure the metabolites from the sap or tissue for determining the plants' responses to various abiotic responses. The phloem and surrounding tissues contain cells associated with synthesizing, distributing, and releasing many significant metabolites involved in the plant's defense mechanism (Killiny and Hijaz 2016). When primary metabolites (such as sugars) are profiled from diseased plant material, many secondary metabolites are thought to interfere with detecting and quantifying the primary metabolites. These interfering compounds may be flavones, flavonoids, phenols, polyphenols, and many other biologically active compounds that are often at elevated levels in infected samples and are likely to increase disease intensity in infected citrus cultivars (Gottwald *et al.*, 2012). To minimize the potential of secondary metabolites to skew the analyses, we examined the global metabolomic profiling of ten different citrus *C*Las-infected cultivars compared to healthy cultivars by using a Liquid chromatography Mass Spectrometer (LC-MS), whereas the degree of infection was determined by using qPCR protocols. This study provides an understanding of how the *C*Las bacterium can eradicate the metabolites which have an important value in plant defense mechanisms. It may also provide the information of source to sink theory of metabolites in plant biology.

MATERIAL AND METHODS
Study background

Leaves of pre-identified healthy and *C*Las-infected citrus cultivars (ten each) were collected from Government Citrus Research Institute (CRI), Tehsil Bhalwal, Sargodha district, Pakistan in fine plastic ziplock bags with area and date of collection (Table 1). The whole study complied with relevant institutional, national, and international guidelines and legislation with appropriate permissions from the Research Institute for the collection of plant specimens at the host institution.

Table 1. Different groups of citrus cultivars under study.

Cultivars	Identification numbers from CR1	Groups
Jaffa	16BR17-C8P1-10	
Hamlin	16FR21-C21P1-5	
Emby Gold	16CR19-C24P1-5	
Casa Grande	16E R23-C19P	
Kozan	16E R9-C16P1-10	Sweet oranges (*Citrus sinensis* L.)
Salustiana	16AR12-C3 P1-10	
Hinckley	16CR13-C18P1-10	
Mars Early	16CR12-C17P1-10	
Tarocco Rose	16AR1-C1 P1-10	
Kinnow	10 ER$-C59 P1-5	Mandarin (*Citrus sinensis* L.)

Both groups of (*C*Las-infected+ Healthy) plants were present in the entirely different zone of different orchard. The trees were matured and fruit-bearing about 3.88m long. The trees which were separated for this experimentation were present in the adjacent row. All trees were approximately the same age of 10−20 years. Maximum, 100-200 (medium size leaves, 5-7cm) symptomatic and healthy leaves were collected per tree and taken to the laboratory for surface sterilization in re-sealable bags.

Starch content analysis by scanning electron microscopy (SEM)

Anatomical modifications of *C*Las infection were detected through the scanning electron microscopy which confirmed the presence of psyllid in the infected leaf. Whereas the absence of bacterium shows the healthy state of citrus leaves. Three replications of root and leaf samples were randomly selected per tree after inoculation from ten *C*Las-infected and an equal number of healthy control trees. The fibrous root was dissected. The root and leaves tissue, by order, was transferred to chilled 100% ethanol for 2 hours. The root samples were then sectioned and stored for 48 h in 100% ethanol. The ethanol solution was refreshed after 24 h. The root and leaves samples were further dehydrated using a Ladd 28000 critical point dryer (Ladd Research Industries, Burlington, VT), subsequently mounted on a stub, and coated with gold/palladium using a Ladd 30800 sputter coater (Ladd Research Industries). Coated tissue samples were observed using a Hitachi S530 SEM (Tokyo, Japan) and photographed using a Cannon Rebel T5i digital camera (Tokyo, Japan). The thickness of the vessel wall, lumen, and starch granules was measured on 10 randomly selected vessels and 10 starch granules per section from both *C*las-infected and control trees. Vessels near the phloem tissue (protoxylem) and pith (metaxylem) were measured in this study. The 2×SE was calculated (Ikram *et al*., 2022).

After anatomical modification, surface sterilization was done by using commercial detergent and 20% Sodium hypochloride (NaOCl) by dipping for 15 minutes. Grinding the plant material, the samples were lyophilized in the host institution and transported to the Microbiology and Cell Sciences Department, University of Florida, Gainesville, FL, USA where the degree of infection was confirmed by using qRT-PCR utilizing SYBR Green (Qunta Biosience, Inc.) (Morgan *et al*., 2012).

qPCR Analysis

Lyophilized leaves of approximately ≤ 200 mg of both group (Healthy + *C*Las-infected) were again disrupted by using mechanical automated shaking (by using automated homogenizer- 2000 Geno/Grinder, Spex CertiPrep) at 1.500 strokes/min for 2 thirty second burst. The removal of RNA has been attained by using RNase; and DNA

extraction was done by using Qiagen protocol (Qiagen Inc., Valencia California) supplied kit. Cells were suspended in TE buffer (1mM EDTA, 10mM Tris-HCL with pH 8.0) of about 100μL. Each DNA sample of 2 μL/25 μL reaction mixture was used for quantification.

The 2 μL of each DNA was used per 25 μL of reaction. Forward and reverse primer set of LJ900 with concentration of 0.6 μM (F) and 1 μM (R) were used (Fig 1b). DNA was annealed at 62°C. The RT-PCR was started at 95°C for about 10 minutes and it was followed by forty cycle at 95°C for 30 seconds, it was annealed at the temperature 62 °C for one min followed by 68 °C for

again one minute. The cycle was terminated at 95 °C for 1 minute, 62 °C for 30 sec and 68 °C for 30 sec (Figure 1a). Fluorescent dye gave the signals which were captured at the end of annealing steps at each 62°C. The reaction specificity was measured by the analysis of thermal melt profiles. Agilent Technologies (Inc. M× 2005 P Fast RT-PCR system) were used for PCR reactions (Figure 1). The threshold values of the reaction cycles were analyzed by using ABI 7500 software (version 2.0.1) with a manually set 0.1 threshold and automated baseline setting (Li *et al.*, 2006; Ledesma-Escobar *et al.,* 2019).
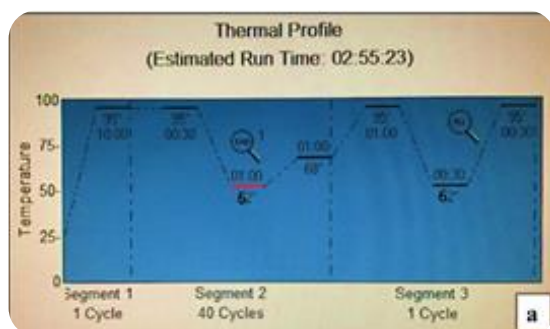
Figure 1. (a): Thermal profile of qRT-PCR for 16S r DNA; (b): Double-stranded amplicon (100bp) of Lj900 (forward and reverse) primer sequence.

Determination of metabolites from LC-MS

This study used the lyophilized leaf samples of ten different cultivars of about ≤ 0.5 g formula weight. The extraction protocol was followed using 1:1 (v: v) of methanol: 10 mM $C_2H_7NO_2$. Pure supernatant was quantified by using LC-MS after vertexing and centrifugation. Two different ion modes were used, i.e., +ive and -ive ion modes. The protocol started with three blanks followed by neat QC. Thermo Q-Exactive Orbitrap Mass Spectrophotometer with Dionex UHPLC and autosampler were used. All samples were quantified using the polarity switching in negative and positive heated ionizing electrospray with a mass resolution of 35,000 at 200 m/z. Metabolite separation was achieved using Angiotensis I-Converting Enzyme6 18-pfp phase 39 B as acetonitrile. Column temperature sets at 25 °C with a 350 μL/min flow rate. About 4 μL pure supernatant of the sample was injected.

Data Processing and statistical analysis

In this study, the Ct values of the *C*Las-infected and healthy citrus varieties were obtained using ABI 7500 software (version 2.0.1). Metabolomic results were presented using Rt and m/z values using Mzmine Cloud. MZmine Cloud (freeware software) was used for the

metabolomic study. The data was characterized by the known and unknown data sets by untargeted predominant data sets that were uncharacterized. In this study, partial least square discriminant analysis (PLS-DA) (2D, 3D, VIP score Plot) plots were used to present the data of metabolites using software Metaboanalyst (www.metaboanalyst.ca/). One-way ANOVA (Welch) and Levene's test used SAS analytical software (SAS Institute Inc., version 9.0) (https://www.sas.com/en_us/softwar/stat.html).

Comparison with post hoc pairwise and Tukey's HSD test was used to compare the mean concentration of metabolites. A heat-map display explained the concentration of each metabolite to construct the similarity of the dendrogram and show the visual differentiation between different metabolites.

RESULTS

The ten different varieties of *Citrus sinensis* and *Citrus reticulate* with visual symptoms of *Candidatus* Liberibacter asiaticus (n=10); and healthy (n=10) with no symptoms were selected from the different fields in this study as shown in (Table 2) (Figures 2A-DZ).

Table 2. Symptoms of Citrus Greening on different cultivars of citrus.

Symptoms of HLB on leaves	Cultivars	Figure 1
Irregular pattern of chlorosis with mottling of leaves, symptoms are similar to nutrient deficiency	Jaffa	A, B, C
	Hamlin	D, E, F
	Emby Gold	G, H, I
	Casa Grande	J, K, L
	Kozan	M, N, O
	Salustiana	P, Q, R
	Hinckley	S, T, U
	Mars Early	V, W, X,
	Tarocco Rose	Y, Z, AZ
Chlorosis, irregular yellowing of leaves, corky and blotchy leaves, similar to Zn deficiency	Kinnow	BZ, CZ, DZ

Figure 2. Different citrus cultivars with Fruit drop (i, iv, vii, x, xiii, xvi, xix, xxii, xxv, xxviii), Vein yellowing-nutrient deficiency leaves (ii, v, viii, xxi, xiv, xvii, xx, xxiii, xxvi, xxix), and Misshapen HLB-symptomatic fruits (iii, xvi, xix, xii, xv, xviii, xxi, xxiv, xxvii, xxx)   Continue…

Figure 2. Different citrus cultivars with Fruit drop (i, iv, vii, x, xiii, xvi, xix, xxii, xxv, xxviii), Vein yellowing-nutrient deficiency leaves (ii, v, viii, xxi, xiv, xvii, xx, xxiii, xxvi, xxix), and Misshapen HLB-symptomatic fruits (iii, xvi, xix, xii, xv, xviii, xxi, xxiv, xxvii, xxx).

Figure 2. Different citrus cultivars with Fruit drop (i, iv, vii, x, xiii, xvi, xix, xxii, xxv, xxviii), Vein yellowing-nutrient deficiency leaves (ii, v, viii, xxi, xiv, xvii, xx, xxiii, xxvi, xxix), and Misshapen HLB-symptomatic fruits (iii, xvi, xix, xii, xv, xviii, xxi, xxiv, xxvii, xxx).

After selecting citrus cultivars, it was testified by obtaining the starch analysis using a spectrophotometer and Scanning Electron Microscopy. Overall, total starch content was higher in HLB-infected citrus leaves than in healthy citrus leaves. It was observed in Table 3 that HLB-infected citrus leaves are statistically different from healthy leaves, with below the highest significant rate of p=0.001. Figure 3 also shows that HLB-infected citrus leaves have higher starch content than healthy leaves. It was observed in Figure 3 that total starch content

($\mu g/mm^2$) was higher in HLB-infected citrus leaves in all citrus varieties as compared to healthy citrus leaves. The highest starch content was observed in the HLB-infected Frost Rose variety, and the lowest value was seen in the healthy Ruby Blood variety. However, the *C*Las-bacterium with phloem plugging was visually seen in Figure 4 using Scanning Electron Microscopy.

After starch analysis, the *C*Las infection status was again checked by using q RT-PCR. Uniformly prepared DNA extracts from citrus cultivars were used for PCR analysis.

Table 3: Analysis of Total Starch content ($\mu g/mm^2$) from healthy and HLB-infected citrus leaves.

Sr. No.	Cultivar name	Total Starch content ($\mu g/mm^2$)		% change
		Infected	Healthy	
1	Kinnow	0.21	0.06	-250.00
2	Frost Rose	0.61	0.05	-1120.00
3	Valencia Late	0.21	0.06	-250.00
4	Hamlin	0.31	0.02	-1450.00
5	Jaffa	0.21	0.03	-600.00
6	Kozan	0.21	0.03	-600.00
7	Taracco	0.30	0.02	-1400.00
8	Ruby Blood	0.20	0.01	-1900.00
9	Musambi	0.32	0.02	-1500.00
10	Blood red	0.20	0.04	-400.00
	Mean	0.278	0.034	
	Std. Deviation	0.1266	0.0178	
	Std. Error Mean	0.0400	0.0056	
	t-test	6.037**		
	Probability	0.001		

Legend: NS = Non-significant (P>0.05); * = Significant (P<0.05); ** = Highly significant (P<0.01); SD = Standard deviation; SE = Standard error
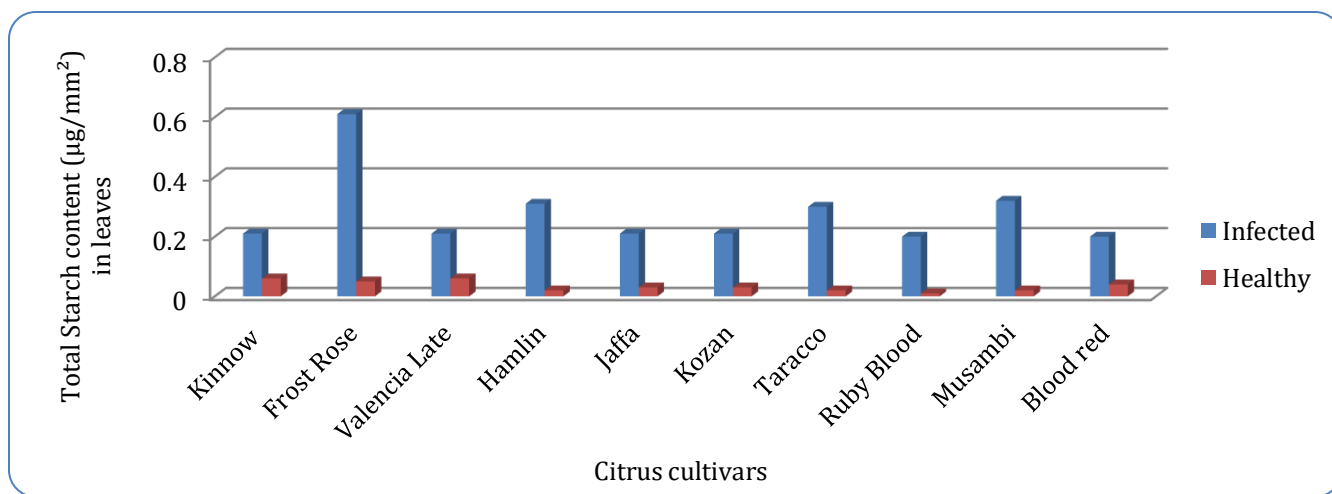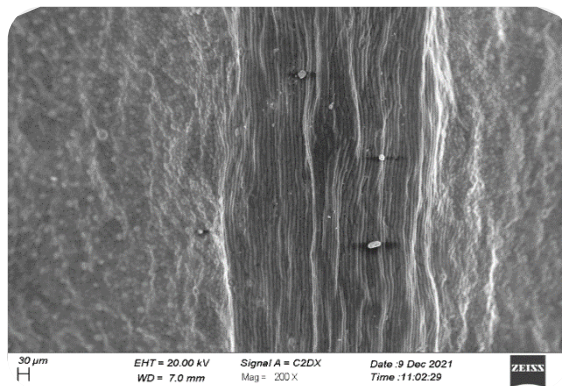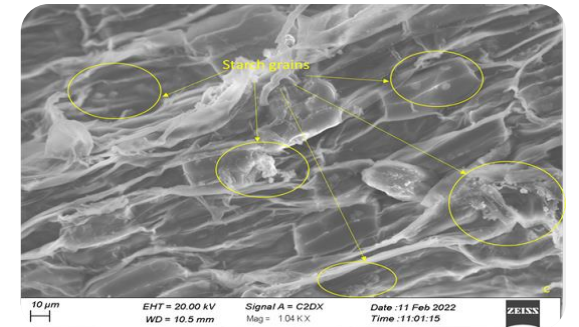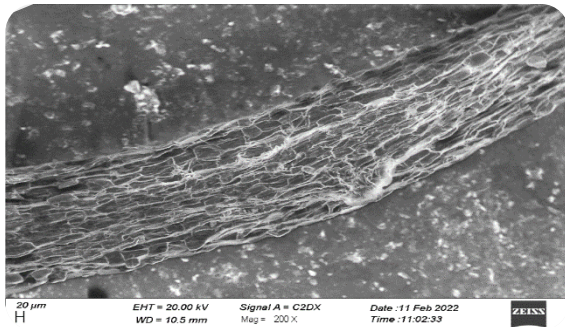

Figure 3. Overall composition of starch content ($\mu g/mm^2$) from healthy and HLB-infected citrus leaves.
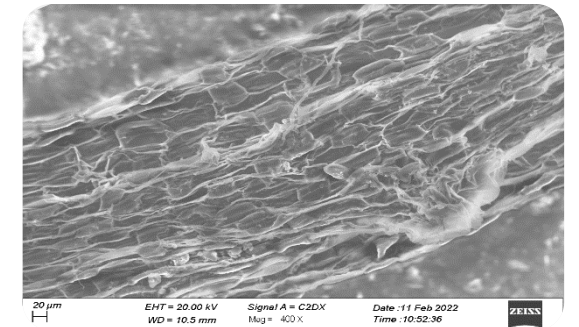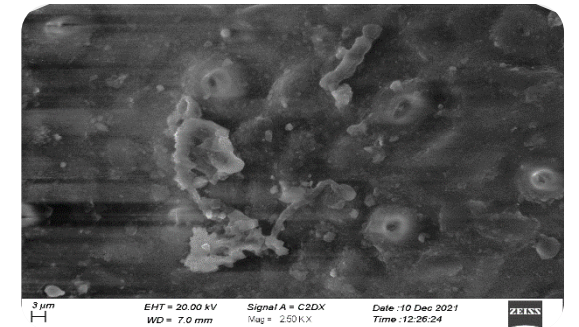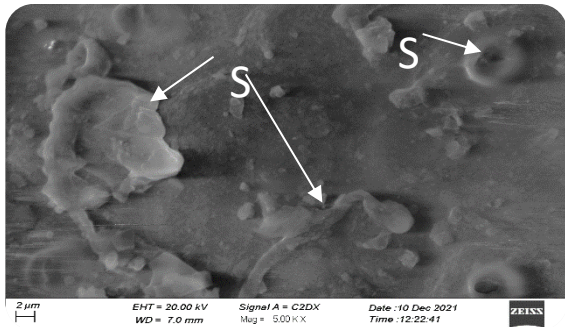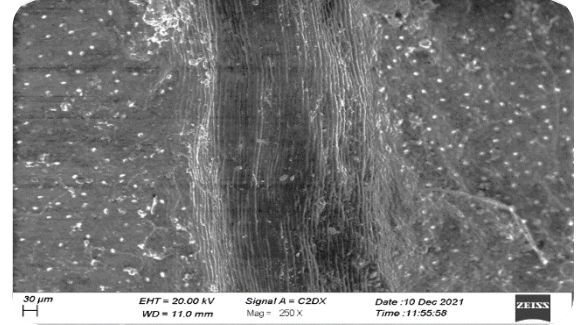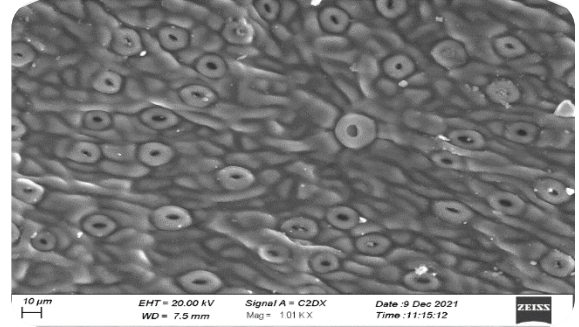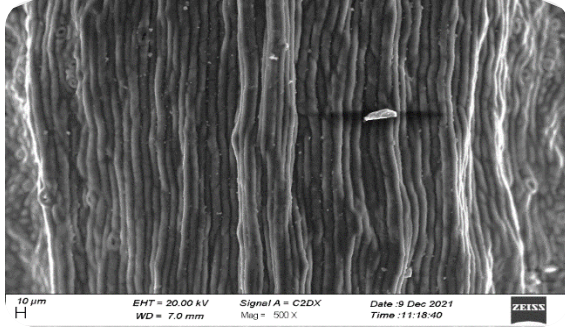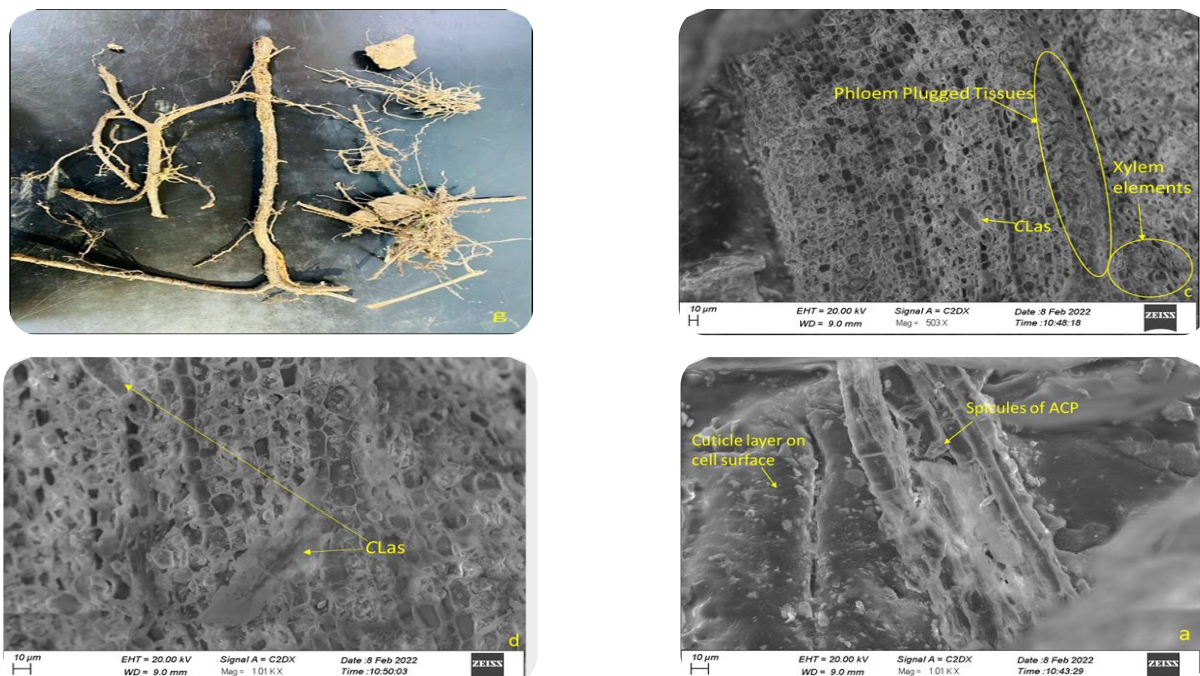
Figure 4. Scanning Electron Microscopy of Kinnow variety; (a) healthy leaves; (b,c) Midrib region (at ×200X and ×500X magnification) shows the normal midrib of healthy leaf containing thick xylem and phloem cells. Morphology of veins (at ×500 X magnification) in healthy leaf showing smooth, tightly packed cells in parallel venation.(d) Anatomy of ventral surface (×500 X and 1.01 KX magnification) of healthy leaf showing normal stomatal opening. e) Infected leaf. (f) Midrib region (at ×250 X magnification) showing much thickened midrib in infected leaf when compared to healthyhighlighted the changes in appearance of infected leaf with starch accumulation due to Huanglongbing disease. It presented the xylem, phloem and parenchymatous cell. (g,h) *C*Las-infected citrus leaf (Kinnow). Anatomy of ventral surface (at ×6.00 KX ×5.00KX, ×2.50KX and ×1.00 KX magnification) of infected leaf with open stomata (Sto) with accumulation of starch granules (SG). (i) Healthy root. (j) Strach granules seen inside the second order of roots cells of healthy Kinnow variety (at Magnification ×400 X). (k) Outer section of second order of healthy (control) Kinnow roots (at Magnification ×200 X). (l) Strach granules seen inside the second order of roots cells of healthy Kinnow variety (at Magnification ×400 X). (m) *C*las-Infected root. (n) *C*Las-infecetd citrus fibrous root of Kinnow showing the *Candidatus* Liberibacter asiaticus (*C*Las) (at ×503 X Magnification) bacterial inside the root cells with depletion of stacrh granules, Ploem plugging is visually seen in cells with xylem cells.(o) Close section of*C*Las-infected citrus fibrous root of Kinnow (at ×1.01 KX Magnification) showing the gram negative, *Candidatus* Liberibacter asiaticus (*C*Las) bacterial inside the root cells with the partial depletion of stacrh granules.(p) *C*Las-infected citrus fibrous root of Kinnow (at ×1.01 KX Magnification showing the spicules of Asian Citrus *Psyllid* (ACP) with partial depleation of starch granules

Figure 5a illustrated a typical calibration curve that correlates the copy number of Candidatus Liberibacter DNA with the Ct value. The copy number of CLas DNA (prophage) was determined by applying a calibration curve prepared by using serial dilution of gel purified amplicon (Figure 5a). The range of Ct values for healthy samples ranged from 15.5 to 36.3 (Table 3). These values correspond to the copy number of the CLas amplicon (prophage-specific) from 0-139. A copy number of 139, or less was considered negative, based on previous studies where no Ct or Ct Value greater than 30 were considered negative and below reliable detection capability (Paula *et al*., 2018; Sieburth *et al*.,

2009). From the symptomatic samples (CLas-Infected), most number values were in the millions, with the highest being 4.5×10^6 (Ct = 16.50). There were three exceptions ranging in copy number from 1.39×10^3 (Ct= 28.2) to 1.87×105 (Ct =21.1). It is noteworthy that the least infected cultivar, Kinnow, had a copy number that was 10- fold higher than the Ct 30- derived value of 139 for the negative threshold. Figure 5b illustrates a typical amplification plot showing three technical replicates for each samples. It was detected the curve showing synthesis of double stranded DNA product (amplicon) where the reaction dynamics are monitored by SYBR™ Green detection of double stranded DNA during RT-PCR

reaction. The HLB infection status was designated either positive (Ct ≤ 30, copy number ≤ 139) or negative based on these results (Table 3). Three of the cultivars, Jaffa, Kinnow, and Hamlin were much less infected than of the remaining 10 cultivars; however, the least infected was

determined to contain 10-times the threshold value (139 copies; Ct = 30), and the other two had copy numbers approximately 100-fold higher than the negative threshold (Paula *et al.*, 2018; Sieburth *et al.*, 2009; Li *et al.*, 2022).
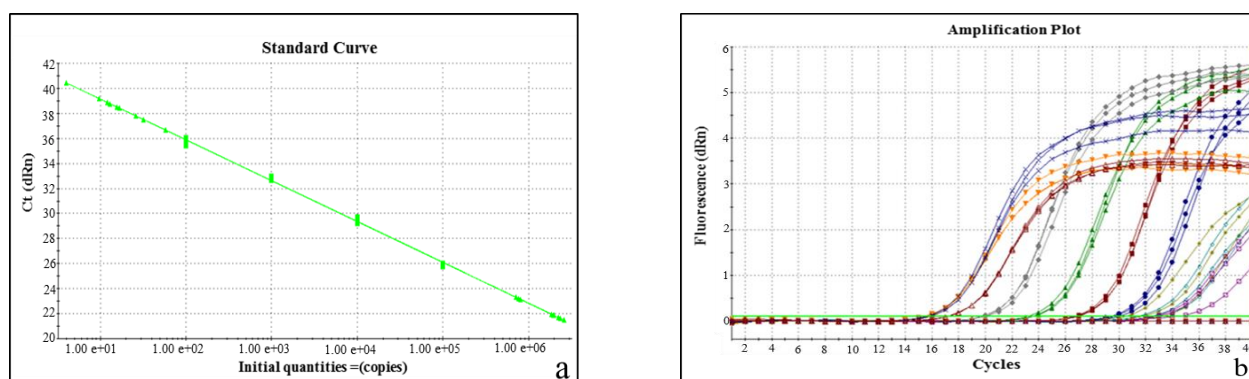

Figure 5. Haunglongbing-infection status in ten citrus cultivars through qPCR.
a) Standard curve of real-time PCR; Squares of the plot (doted lines) = Calibration values, Triangles (Green due to SYBR® Green) = Unknown samples, linear regression formula: Y=-3.3261 x LOG(X)+36.40, Rsq: 0.995, efficiency of the amplification=102%; b) Typical amplification plot of 3 replicates per sample from HLB positive and healthy plant samples obtained from real-time PCR.

Global Analysis for the determination of metabolites

Results of LC-MS were compared with MZmine (freeware) to identify and align features and fill the gaps to add any missed features of the first alignment algorithm. According to the volcano plot, a negligible count of known metabolites was taken from the stock, but various components were left uncharacterized. The differences in the total metabolites between healthy and HLB-Infected leaves include local variations in pigment distribution over the leaf surfaces. Although there were large numbers of unknown metabolites, varying levels of known amino acids are of interest. The main difference in this research depended on the positive and negative ion modes. There were two main groups present in this study i.e., healthy and HLB-infected. The Volcano Plot, PLS-DA, permutation test, and Heat map analysis represented unique differences in healthy and *C*Las-infected groups. The data set of LC-MS analysis represented the known and unknown features (metabolites) which separates the healthy from-infected citrus cultivars. The major categories of metabolites were not known in this study previously. About 287 known metabolites were explained from the negative ion mode whereas 213 known metabolites were identified from the positive ion database, which were

explained in the following section.

Negative ion mode

Outcomes of the study suggested that there were numerous variations that were recorded in both infected and healthy leaves (Figure 6 (a) and (b)), which enhanced the chances of separations of the data set which is not based on two marked classes (positive and negative ions), for further confirmational studies 2D and 3D scores plots were used (Figure 6(c) and(d)). There were numerous metabolites with VIP scores above 1 (Figure 6 e). However, it appeared that PLS-DA had overfitted the data as per the permutation test(p=0.25) which proved that the infection status of the leaves was random because 25% of the permutations resulted in good separations. A low significance score on the permutation test indicated that separation has only a 75% chance of being dependent on the HLB infection status (Figure 6 f), further classification of the data was done through Heat maps (Figure 6 g-i) (Table 5). Several substances, including Oxalosuccinic acid, L-methionine, glyceraldehyde, and 3-hydroxydecanoic acid, exhibited significant increases of at least four-fold. Additionally, glycolate and eujambolin also showed increased levels. Notably, only approximately half of the tested chemicals demonstrated statistically significant changes.

Table 4. Mean Ct Value, Average concentration of DNA, and copy number in different citrus cultivars through qPCR analysis.

Citrus Cultivars	Mean Ct Values		Average Copies of DNA	
	Healthy leaves	Infected leaves	Healthy leaves	Infected leaves
Jaffa	0	2.11E+01	0	1.87E+05
Kinnow	3.63E+01	2.82E+01	1.39E+01	1.39E+03
Hamlin	0	2.16E+01	0	1.32E+05
Emby Gold	0	1.83E+01	0	1.35E+06
Casa Grande	0	1.79E+01	0	1.71E+06
Kozan	3.68E+01	1.78E+01	9.78E+00	1.86E+06
Salustiana	0	1.75E+01	0	2.30E+06
Hinkeley	0	1.87E+01	0	9.91E+05
Mars Early	0	1.73E+01	0	2.89E+06
Tarocco Rose	0	1.70E+01	0	3.24E+06
Tarocco-Nucellar	0	1.65E+01	0	4.50E+06
Frost Rose	0	1.75E+01	0	2.47E+06
Ruby Blood	3.67E+01	1.96E+01	1.33E+01	9.91E+05
Blood Red	0	1.78E+01	0	1.86E+06
New Hall	3.69E+01	1.55E+01	1.18E+01	1.46E+06

Positive ion mode

A PLS-DA overview Plot showed that PC1 and PC2 provided good separation of features. Significant fold changes were seen in the Volcano score plot of known metabolites (positive ions) of *C*Las-tolerant (Infected) leaves. Many metabolites, i.e., Arachidonic acid, Methionine, Leucine, Citrulline, and Cytosine of *C*Las-infected leaves, have higher concentrations than healthy leaves. Furthermore, many known compounds, i.e., Nicotinamide, Asparagine, Caffeate, Glutarate, Raffinose, and Ergothioneine, have decreased concentrations in *C*Las-infected leaves compared to healthy leaves (Figure 6 A), which was further assessed through 2D (Figure 6 B), and 3D Scores Plots (Figure 6 C) and results were satisfactory. Moreover, numerous metabolites significantly contributed to the VIP Plot analysis (Figure 6 D). However, the reduced level of significance on the permutation test indicated that

separation has only a 75% chance of being dependent on the HLB infection status (Figure 6 E). Inspection of the heat Map indicated great variability in the relative strength of metabolites (Figure 6 F-G) (Table 5).

Results of the present study highlighted various differences in metabolic profiles among both diseased and healthy experimental samples, with variation in the colors and the presence of pigments that were visible to the unaided eye, but to large numbers of metabolites. Volcano plot analysis was found to be very effective in highlighting the differences in negative and positive ion composition and relative abundance of all samples, which were further supported by statistical tools. Furthermore, PLS-DA and heat map plots indicated a unique pattern of differences in a mixture of approximately 500 known and 8,000 unknown metabolites associated with healthy and symptomatic leaves.
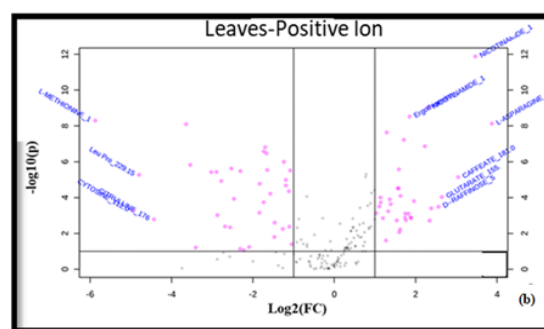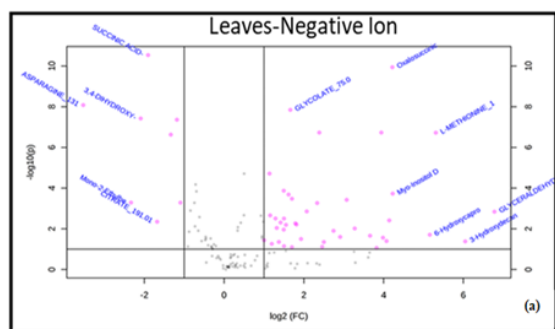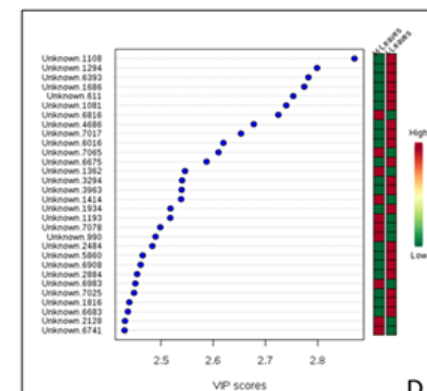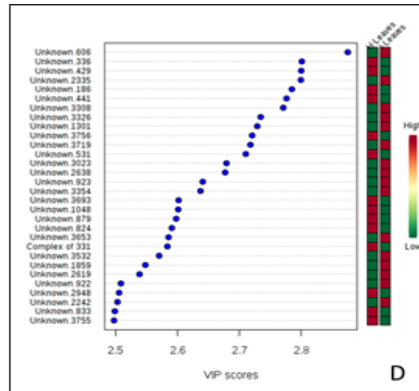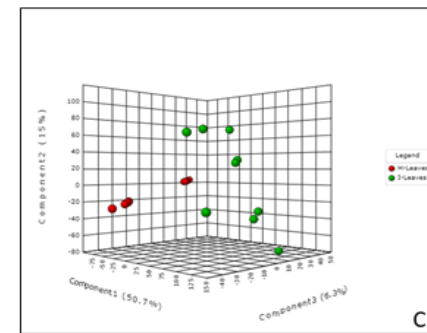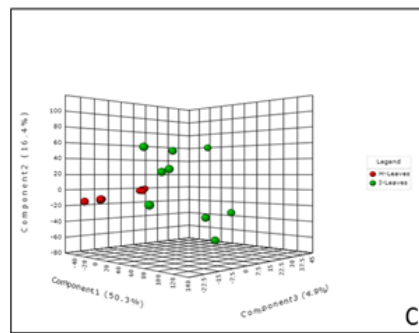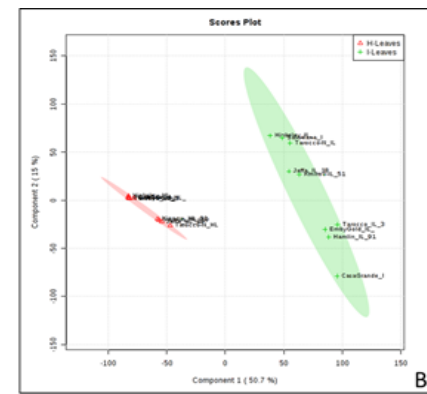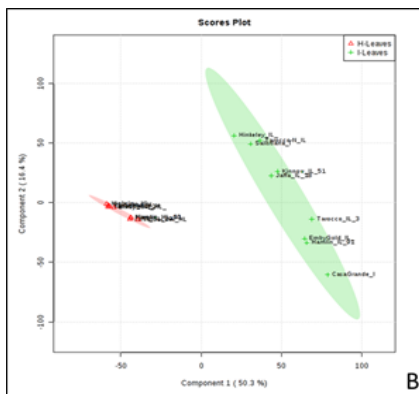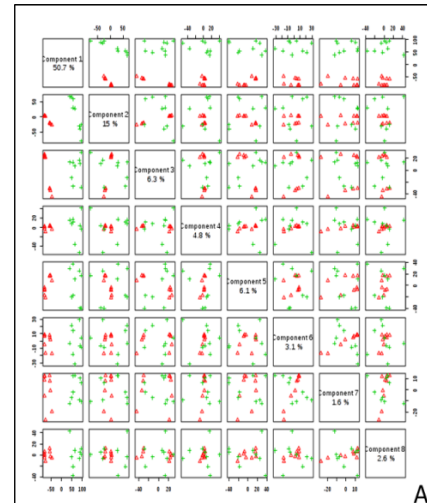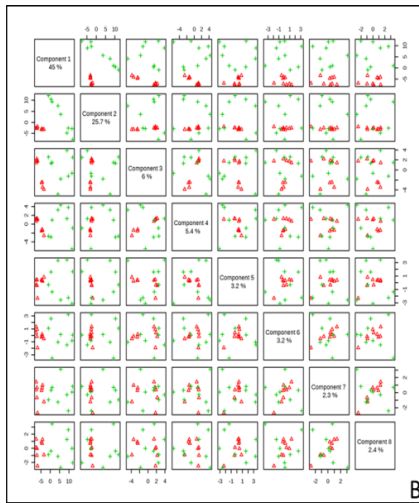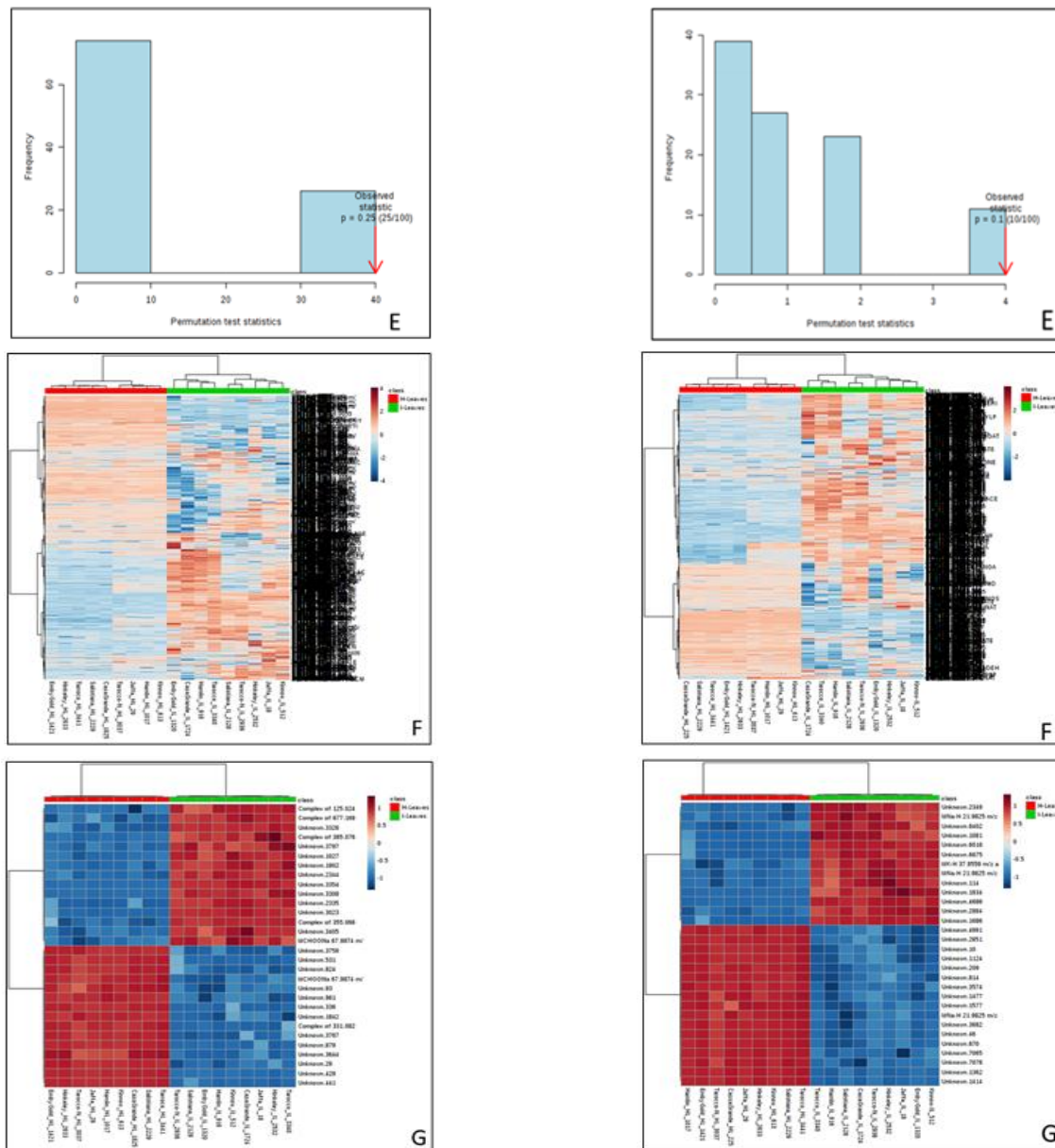
Figure 6. Metabolomic analysis of from healthy and HLB-affected leaves only. Volcano plot of fold-changes in metabolites [(a) Negative Ions (small alphabetical letters) (b) positive ions (capital alphabetical letter)] versus probability. Variations detected during study suggested the clear-cut differences among both healthy and diseased samples. Pink dots> 2-fold change at > 95% significance (p<0.05); Black dots are below the threshold for change or significance. (Table 5). PLSA-DA score plot of negative ions and Positive ions: (c, A) Overview plot, (d, B) 2D plot, (e, C) 3D plot, (f, D) VIP plot, (g, E) Permutation test score plot, p= 0.1. Heat maps of (h, F) Total unknowns plus known metabolites, (i, G) Top 30 changes.

Table 5. Estimation of probabilities for known and unknown metabolites.

Classes of compounds	Metabolites of Healthy and HLB-infected citrus leaves							
	Negative ion mode (Mean ± SD)				Positive ion mode (Mean ± SD)			
	Metabolites	Healthy	Infected	Tukey Pr>|t|	Metabolites	Healthy	Infected	Tukey Pr>|t|
Amino acids	3,4-Dihydroxy-L-Phenylalanine*	0.02 ± 0.01	0.01 ± 0.00	<.0001	1-Aminocyclopropane-1-Carboxylate	2.32 ± 0.20	2.67 ± 0.68	<0.1859
	Asparagine*	20.77 ± 2.76	1.84 ± 1.58	<.0001	1-Hexanesulfonic acid	0.01 ± 0.00	0.01 ± 0.00	<.0001
	Aspartate	3.73 ±0.68	7.66 ± 7.01	<0.1137	2-Aminophenol	0.04 ± 0.01	0.05 ± 0.01	<0.8242
	BoC-L-Tyrosine	4.42 ± 0.50	4.85 ±1.43	<0.3988	2-Hydroxyphenylalanine	4.34 ± 1.06	10.65 ± 3.89	<0.0005
	L-Arginine	1.54 ± 0.15	2.27 ± 2.95	<0.4720	3-Amino-4-Hydrobenzoic Acid	0.29± 0.14	0.42 ± 0.52	<0.5061
	L-Glutamic Acid	11.93 ± 1.12	9.66 ± 8.42	<0.4345	3-Amino-5-Hydrobenzoic Acid	0.01 ± 0.01	0.04 ± 0.02	<0.0017
	L-Glutamine	2.15 ± 0.28	3.09 ±1.84	<0.1485	3-Nitro-L-Tyrosine	0.01 ± 0.00	0.02 ± 0.02	<0.0636
	L-Isoleucine*	0.03 ± 0.02	0.17 ±0.12	<0.0036	3,4-Dihydroxy-L-Phenylalanine	0.12 ± 0.03	0.25 ± 0.05	<.0001
	L-Methionine*	0.01 ± 0.01	0.31 ± 0.34	<0.0162	4-AminobutanoateGABA	0.72 ± 0.04	0.39 ± 0.15	<.0001
	L-Serine*	4.92 ± 1.69	2.71 ±.70	<0.0136	4-Guanidinobutanoate	1.00 ± 0.10	2.18 ± 1.12	<0.0100
	L-Tyrosine*	0.26 ± 0.05	0.86 ± 0.38	<0.0003	5-Aminolevulinic Acid	0.05 ± 0.03	0.04 ± 0.02	<0.2184
	L-Valine*	0.26 ± 0.05	0.86 ± 0.38	<0.0003	5-Hydroxy-L-Trytophan	0.07 ± 0.01	0.03 ± 0.01	<.0001
	N-Acetyl-DL-Glutamic Acid	0.16 ± 0.01	0.17 ±0.08	<0.6362	5-Hydroxy-N-formylkynurenine	0.05 ± 0.03	0.04 ± 0.02	<0.2184
	N-Acetyl-glycine	0.14 ± 0.01	0.16 ± 0.10	<0.6113	5-Oxo-L-Proline	0.54 ± 0.18	0.65 ± 0.45	<0.5121
	N-Acetyl-L-Alanine*	0.39 ± 0.03	0.26 ± 0.10	<0.0018	6-Hydroxynicotinate	0.01 ± 0.00	0.00 ± 0.00	<0.2707
	N-Acetyl-L-Phenylalanine*	1.37 ± 0.02	0.87 ± 0.29	<.0001	Acetaminophen/Paracetamol	0.01 ±0.02	0.01 ± 0.00	<0.3747
	N-Butoxycarbonyl-L-Aspartic Acid	0.01 ± 0.01	0.01 ± 0.00	<0.9277	Alanine/Sarcosine	7.64 ± 1.63	19.34 ± 6.70	<0.0002
	N- Butoxycarbonyl -L-tert-Leucine	0.01 ± 0.01	0.01 ± 0.01	<0.0521	Alpha-Aminoadipate/N-Methyl-L-Glutamate	1.08 ± 0.09	0.23 ± 0.10	<.0001
	N- Butoxycarbonyl -L-Tryptophan	0.92 ± 0.12	0.98 ± 0.29	<0.6509	Aspartate	4.53 ± 0.88	6.89 ± 5.96	<0.2866
	Proline*	0.58 ± 0.08	1.13 ± 0.51	<0.0058	Betaine	9.23 ± 3.60	30.50 ± 14.60	<0.0012
	Sarcosine/Beta-Alanine	0.13 ± 0.03	0.27 ± 0.22	<0.0748	Tert-Butoxycarbonyl-D-Phenylalanine	4.47 0.57	3.39 ± 1.06	<0.0208
	Taurine*	359.61±22.43	203.73 89.34	<0.0001	Tert-Butoxycarbonyl-L-Tyrosine	2.86 ± 0.51	2.17 ± 0.75	<0.0452
	Threonine/Homoserine*	3.21 ± 0.32	8.12 ±5.28	<0.0133	Caffeate	1.12 ± 0.12	0.14 ± 0.19	<.0001
	Tryptophan	3.98 ± 0.45	5.36 ± 3.63	<0.2733	Caffeine 13C	0.74 ± 0.03	0.68 ± 0.20	<0.3740
	-	-	-	-	Caffeine D3	0.30 ± 0.02	0.29 ± 0.08	<0.9400
	-	-	-	-	Citrulline	0.19 ± 0.08	4.51 ± 5.76	<0.0518

-	-	-	-	Creatine-D3	0.08 ± 0.07	0.10 ± 0.06	<0.5470
-	-	-	-	Creatinine	0.00 ± 0.00	0.04 ± 0.11	<0.3734
-	-	-	-	Diethyl-2-Methyl-3-Oxosuccinate	0.42 ± 0.14	0.32 ± 0.32	<0.4375
-	-	-	-	Diphenylamine	0.01 ± 0.01	0.01 ± 0.00	<0.9530
-	-	-	-	Ergothioneine	0.06 ± 0.02	0.05 ± 0.01	<0.0341
-	-	-	-	Formylkynurenine	0.06 ± 0.02	0.05 ± 0.01	<0.0341
-	-	-	-	Glucosamine/Mannosamine	2.73 ± 0.80	3.73 ± 3.93	<0.4917
-	-	-	-	Glutarate	0.02 ± 0.00	0.00 ± 0.00	<.0001
-	-	-	-	Glycine	0.24 ± 0.24	3.21 ± 1.50	<.0001
-	-	-	-	Glycyl-L-leucine	0.24 ± 0.24	3.21 ± 1.50	<.0001
-	-	-	-	Hippuric Acid	0.01 ± 0.01	0.01 ± 0.00	<0.7712
-	-	-	-	Kynuramine	0.01 ± 0.00	0.00 ± 0.00	<0.0580
-	-	-	-	Kynurenic Acid	0.18 ± 0.02	0.18 ± 0.14	<0.9983
-	-	-	-	L-Arginine	57.41± 4.57	40.47 ± 43.38	<0.2906
-	-	-	-	L-Asparagine	84.78±11.3	5.72 ± 3.37	<.0001
-	-	-	-	N-Acetyl-L-Leucine	0.00 ± 0.00	0.01 ± 0.00	<0.1903
-	-	-	-	N-Acetylneuraminate	0.10 ± 0.02	0.10 ± 0.08	<0.7473
-	-	-	-	N-Acetylputrescine	0.22 ± 0.01	0.25 ± 0.14	<0.5736
-	-	-	-	N-Acetylserotonin	0.023± 0.00	0.03 ± 0.08	<0.8498
-	-	-	-	N-(tert-Butoxycarbonyl) -L-Aspartic Acid	0.39 ± 0.03	0.18 ± 0.09	<.0001
-	-	-	-	N-(tert-Butoxycarbonyl)-L-Tryptophan	0.39 ± 0.06	0.31 ± 0.09	<0.0400
-	-	-	-	N-Methyl-D-Aspartic Acid	8.26 ± 2.27	52.39 ± 31.15	<0.0012
-	-	-	-	Pantothenic Acid	1.33 ± 0.07	1.33 ± 0.46	<0.9957
-	-	-	-	Pyridoxal	0.19 ± 0.03	0.07 ± 0.06	<.0001
-	-	-	-	Pyridoxine	0.46 ± 0.12	1.19 ± 0.65	<0.0071
-	-	-	-	Quinate	1.23 ± 0.13	0.48 ± 0.28	<.0001
-	-	-	-	S-Dihydroorotate	0.01 ± 0.00	0.00 ± 0.00	<.0001
-	-	-	-	Serotonin	0.03 ± 0.01	0.01 ± 0.01	<0.0024
-	-	-	-	Serotonin-NH_3	0.03 ± 0.00	0.18 ± 0.22	<0.0654
-	-	-	-	Threonine/Homoserine	22.37± 1.01	28.24 ± 5.86	<0.0138
-	-	-	-	Tryptophan	50.81± 6.18	39.04 ± 12.37	<0.0282
-	-	-	-	Tryptophan-2,3,3-D3	1.29 ± 0.07	1.05 ± 0.29	<0.0389
-	-	-	-	Tryptophan-NH_3	19.82± 2.38	15.29 ± 4.87	<0.0309
-	-	-	-	Tyramine	0.31 ± 0.04	2.03 ± 3.15	<0.1455
-	-	-	-	L-Carnitine	0.21 ± 0.16	0.14 ±0.04	<0.2210
-	-	-	-	L-Glutamine	49.42± 1.77	30.92 ±	<0.0027

					14.45		
-	-	-	-	L-Histidine	6.70 ±0,72	7.73 ± 4.58	<0.5419
-	-	-	-	L-Isoleucine	9.40 ± 6.72	52.76 ± 19.75	<0.0001
-	-	-	-	L-Kynurenine	0.02 ± 0.00	0.02 ± 0.01	<0.9842
-	-	-	-	L-Leucine-D10	0.08 ± 0.01	0.08 ± 0.03	<0.6573
-	-	-	-	L-Methionine	0.09 ± 0.05	5.71 ± 5.36	<0.0099
-	-	-	-	L-Proline	341.74±12	349.44±102.5	<0.8363
-	-	-	-	L-Serine	16.00± 1.38	6.31 ± 3.19	<.0001
-	-	-	-	Leu Pro	16.00± 1.38	6.31 ± 3.19	<.0001
-	-	-	-	Leucine	0.11 ± 0.08	3.71 ± 3.88	<0.0197
-	-	-	-	LL-2,6-Diamino heptanedioate	6.56 ± 7.21	51.69 ± 19.20	<.0001
-	-	-	-	Urocanate	0.03 ± 0.01	0.24 ± 0.17	<0.0035
-	-	-	-	3-Hydroxy-3-Methyl Gluterate	0.02 ± 0.00	0.06 ± 0.03	<0.0020
Carboxylic Acid	2',4'-Dihydroxyacetophenone*	0.32 ± 0.01	0.21 ± 0.13	<0.0215	4-Hydroxybenzoate	0.15 ± 0.01	0.12 ± 0.02	<0.0098
	Quinate*	359.61±22.4	203.73±89.3	<0.0001	4-Imidazoleacetic Acid	0.18 ± 0.03	0.12 ± 0.04	<0.0054
	Methyl-2-Oxovaleric Acid*	0.06 ± 0.04	0.21 ± 0.14	<0.0074	Anthranilate	0.02 ± 0.00	0.08 ± 0.13	<0.1883
	Citramalate*	2.41 ± 0.14	3.47 ± 0.81	<0.0014	Lauroylcarnitine	0.01 ± 0.01	0.00 ± 0.00	<0.0032
	Kynurenic Acid	0.22 ± 0.02	0.27 ± 0.21	<0.4192	Methylmalonate	0.01 ± 0.00	0.01 ± 0.01	<0.2158
	3,4-Dihydroxyphenulacetate	0.13 ± 0.01	0.09 ±0.08	<0.2081	R-Malate	1.27 ± 0.06	1.30 ± 1.66	<0.9581
	3-Dehydroshikimate	0.27 ± 0.04	1.42 ± 3.26	<0.3078	Succinate	0.05 ± 0.01	0.43 ± 0.36	<0.0098
	3-Hydroxy-3-MethylGluterate*	0.29 ± 0.03	0.89 ± 0.54	<0.0042	Arachadonic acid	0.02 ± 0.00	0.22 ± 0.12	<0.0003
	3-Hydroxydecanoic acid	0.02 ± 0.01	1.14 ± 1.62	<0.0539	-	-	-	-
	3-Hydroxyphenylacetate*	0.32 ± 0.05	0.23 ± 0.10	<0.0482	-	-	-	-
	4-Hydroxyphenylacetate	0.17 ± 0.15	0.37 ± 0.43	<0.2207	-	-	-	-
	4-oxoproline*	0.26 ± 0.07	0.63 ±0.49	<0.0419	-	-	-	-
	6-Carboxyhexanoate	0.03 ± 0.01	0.04 ± 0.02	<0.1351	-	-	-	-
	Citrate*	89.11 ± 5.00	28.80± 19.58	<.0001	-	-	-	-
	D-Sacchric Acid*	191.30±13.9	279.08±49.5	<0.0001	-	-	-	-
	Fumaric Acid	0.36 ± 0.23	1.37 ± 1.50	<0.0631	-	-	-	-
	Malate	108.18±7.45	129.68±14	<0.6295	-	-	-	-
	Mono-2-Ethylhexyl Phthalate	0.10 ± 0.01	0.10 ± 0.02	<0.9175	-	-	-	-

Category	Compound				Compound			
	Oxalosuccinic Acid*	0.04 ± 0.01	0.84 ± 0.38	<.0001	-	-	-	-
	Succinate*	6.62 ± 1.74	44.41± 43.01	<0.0180	-	-	-	-
	Tartaric Acid	1.59 ± 0.06	1.54 ± 0.39	<0.6620	-	-	-	-
Organic acids	2-Hydroxy-4-Methylthiobutyric Acid	0.28 ± 0.03	0.20 ± 0.28	<0.4429	10-Hydroxydecanoate	0.01 ± 0.00	0.04 ± 0.03	<0.0244
	3-(2-Hydroxyphenyl) propanoate	0.06 ± 0.01	0.07 ± 0.06	<0.6112	3-2-Hydroxyphenyl Propanoate	0.05 ± 0.00	0.04 ± 0.03	<0.3987
	3-tert-Butyladipic acid*	0.23 ± 0.05	0.47 ± 0.19	<0.0020	3-Uredopropionate	0.04 ± 0.00	0.12 ± 0.22	<0.3204
	3-Uredioprppionate	0.02 ± 0.01	0.01 ± 0.19	<0.2255	3,4-Dimethylbenzoic acid	0.03 ± 0.01	0.02 ± 0.00	<0.0022
	4-Dodecylbenzenesulfonate	2.20 ± 0.74	2.75 ± 1.63	<0.3720	3,5-Di-tert-butylbenzaldehyde	0.13 ± 0.01	0.09 ± 0.02	<0.0004
	Alpha-Ketoglutaric Acid	0.57 ± 0.10	0.45 ± 0.24	<0.1707	4-Hydroxy-L-Phenylglycine	0.20 ± 0.04	0.18 ± 0.23	<0.8711
	Ascorbic acid	0.08 ± 0.02	0.64 ± 0.96	<0.0934	5-Hydroxymethyl-2-furaldehyde	2.22 ± 0.46	2.39 ± 2.89	<0.8691
	Caffeate	0.04 ± 0.01	0.03 ± 0.02	<0.4268	Citramalate	0.04 ± 0.00	0.05 ± 0.02	<0.2057
	Caffeic Acid*	0.08 ± 0.02	0.05 ± 0.03	<0.0226	α-Ketoglutaric Acid	0.022	0.03 ± 0.03	<0.6279
	D-Glucuronic Acid/D-Glucurono Lactone/D-Galacturonic Acid_	9.05 ± 0.85	7.33 ±2.43	<0.0629	Bis 2-ethylhexyl phthalate	0.44 ± 0.01	0.42 ± 0.14	<0.8069
	Ethulmalonic Acid	0.86 ± 0.06	1.49 ± 1.12	<0.1135	Camphor_153.1271_9.97	0.09 ± 0.01	0.05 ± 0.03	<0.0014
	Ferulate*	0.43 ± 0.02	0.26 ± 0.11	<0.0003	Choline	120.36±7.6	91.12 ± 40.45	<0.0632
	Gluconic Acid/D-Gulonic Acid Gama-Lactone*	105.64 ± 5.91	65.88 ± 17.74	<.0001	Dibutyl adipate	0.00 ± 0.00	0.00 ± 0.00	<0.0623
	Gluterate *	0.28 ± 0.03	0.11 ± 0.03	<.0001	Dibutyl phthalate	0.14 ± 0.04	0.09 ± 0.03	<0.0258
	Glyceraldehyde/Lactate*	0.64 ±0.33	70.17± 76.58	<0.0150	Dipropylene Glycol	0.04 ± 0.01	0.04 ± 0.02	<0.7931
	Glycolate*	0.76 ±0.11	2.48 ± 0.81	<.0001	Dipropylene Glycol dibenzoate	0.01 ± 0.00	0.01 ± 0.00	<0.5406
	Glyoxilic Acid*	0.22 ± 0.03	0.64 ± 0.47	<0.0173	Dopamine	0.04 ± 0.00	0.02 ± 0.01	<.0001
	Homovallinate	0.11 ± 0.05	1.08 ± 1.30	<0.0403	Erucamide	0.37 ± 0.03	0.30 ± 0.08	<0.0489
	3-Amino-4-HydroxyBenzoic acid	0.03 ± 0.01	0.13 ± 0.19	<0.1227	Gallic Acid	0.00 ± 0.00	0.00 ± 0.00	<.0001
	Xanthauric acid	0.40 ±0.34	1.29 ± 1.66	<0.1359	Garcinia lactone dibutyl ester	0.18 ± 0.08	0.23 ± 0.09	<0.3486
	3-Aminosalicylic acid	0.32 ± 0.15	0.26 ± 0.18	<0.4691	Glutathione Disulfide	0.32 ± 0.02	0.08 ± 0.15	<0.0004
	3-methyladipic acid	0.19 ± 0.02	0.17 ± 0.12	<0.6891	Isocitric Acid	0.09 ± 0.01	0.06 ± 0.02	<0.0020
	4-Methyl-2-Oxo-Pentanoic Acid*	0.14 ± 0.02	0.37 ± 0.23	<0.008	Isovaleryl carnitine	0.02 ± 0.01	0.01 ± 0.01	<0.1536
	5-Hydroxyindoleacetate	0.08 ± 0.01	0.44 ± 0.54	<0.0581	L-Acetyl carnitine	0.01 ± 0.00	0.01 ± 0.01	<0.1697
	6-Phosphogluconic Acid	0.74 ± 0.20	1.61 ± 1.75	<0.8267	Lysophosphatidylethanolamine160	0.07 ± 0.02	0.01 ± 0.02	<.0001
	Nicotinate*	0.13 ± 0.03	0.25 ± 0.12	<0.0089	1-Palmitoyl-sn-glycero-3-phosphocholine161	0.00 ± 0.00	0.00 ± 0.01	<0.4331

Category	Metabolite	Value 1	Value 2	p	Metabolite	Value 1	Value 2	p
	Phenylpyruvate	0.26 ± 0.02	0.22 ± 0.18	<0.5218	1-Palmitoyl-sn-glycero-3-phosphocholine180	0.00 ± 0.00	0.00 ± 0.00	<0.0002
	Phosphocholine*	0.21 ± 0.05	0.29 ± 0.05	<0.0030	1-Palmitoyl-sn-glycero-3-phosphocholine 181	0.00 ± 0.00	0.00 ± 0.01	<0.9723
	Pimelic Acid	0.00 ± 0.00	0.05 ± 0.13	<0.2989	1-Palmitoyl-sn-glycero-3-phosphocholine182	0.01 ± 0.00	0.00 ± 0.04	<0.6277
	Shikimate	0.55 ± 0.08	0.64 ± 0.99	<0.7824	Lysophosphatidylethanolamine 180	0.00 ± 0.00	0.00 ± 0.00	<0.5247
	Xanthurenic Acid*	0.16 ± 0.04	1.57 ± 1.73	<0.0269	Lysophosphatidylethanolamine181	0.00 ± 0.00	0.018 ± 0.02	<0.0940
	-	-	-	-	Methyl Beta-D-Galactoside	0.07 ± 0.01	0.04 ± 0.02	<0.0023
	-	-	-	-	Monobutyl phthalate	0.03 ± 0.00	0.02 ± 0.01	<0.0035
	-	-	-	-	N-Butyl benzene Sulfonamide	0.01 ± 0.00	0.01 ± 0.00	<0.0595
	-	-	-	-	Nicotinamide	0.30 ± 0.04	0.03 ± 0.01	<.0001
	-	-	-	-	O-Succinyl-L-Homoserine	0.01 ± 0.00	0.01 ± 0.01	<0.9421
	-	-	-	-	Orthophosphate	0.52 ± 0.05	0.39 ± 0.36	<0.3129
	-	-	-	-	Polyethyleneglycol-N5	0.06 ± 0.01	0.03 ± 0.01	<0.0002
	-	-	-	-	Phenethylamine	0.11 ± 0.01	0.10 ± 0.03	<0.1918
	-	-	-	-	Phenylalanine	99.77 ±7.45	60.69 ± 18.53	<0.0001
	-	-	-	-	Phenylalanine-HCOOH	19.92 ± 1.6	12.19 ± 3.73	<.0001
	-	-	-	-	Picolinic Acid_124.0394_1.28	1.07 ± 0.28	2.13 ± 0.94	<0.0082
	-	-	-	-	Pipecolate/L-Pipecolic Acid	0.55 ± 0.10	0.90 ± 0.66	<0.1571
	-	-	-	-	Proprionyl carnitine	0.01 ± 0.00	0.01 ± 0.01	<0.0658
	-	-	-	-	Ptelatoside A	0.02 ± 0.00	0.03 ± 0.01	<0.3011
	-	-	-	-	Shikimate	0.00 ± 0.00	0.00 ± 0.00	<0.0170
					OA-Starch acetate	0.01 ± 0.00	0.03 ± 0.01	<.0001
Phenols	3-(4-hydroxyphenyl) lactate*	0.04 ± 0.01	0.12 ± 0.10	<0.0319	OA-Sulcatol	0.02 ± 0.02	0.01 ± 0.00	<0.0234
	Pyridoxine*	0.05 ± 0.01	0.16 ± 0.13	<0.0291	OA-Syringic Acid	0.02 ± 0.00	0.02 ± 0.01	<0.0088
	Mevalonolectone	0.11 ± 0.01	0.36 ± 0.40	<0.0733	Tetrahydrothiophene-1-oxide	0.03 ± 0.00	0.03 ± 0.02	<0.5868
	Monobutyl phthalate	0.03 ± 0.00	0.04 ± 0.02	<0.2632	Trans-Cinnamaldehyde	0.21 ± 0.02	0.25 ± 0.08	<0.1423
	Hydroquinone	0.27 ± 0.22	0.94 ± 1.25	<0.1368	OA-Trans-Cinnamate	0.21 ± 0.02	0.25 ± 0.08	<0.1423
	-	-	-	-	Triethyl phosphate	0.06 ± 0.02	0.06 ± 0.02	<0.6075
	-	-	-	-	Trigonelline	7.35 ± 1.08	4.18 ± 1.43	<0.0001
	-	-	-	-	Xanthurenic Acid	0.48 ± 0.09	1.41 ± 1.41	<0.0565
	-	-	-	-	Homogentisate	0.11 ± 0.00	0.03 ± 0.01	<.0001
	-	-	-	-	Biotin	0.00 ± 0.00	0.02 ± 0.01	<0.0033
Carbohydrates/Sugars	2-deoxy-D-galactose fructose/glucose*	0.07 ± 0.00	0.20 ± 0.16	<0.0244	6C-Sugar Alcohol	0.11 ± 0.06	0.56 ± 0.68	<0.0836
	Disaccharide GLC/GLC-FRC/GAL-GLC*	4.94 ± 0.26	6.41 ± 1.25	<0.0032	Aldo/Keto Hexose	1.24 ± 0.35	2.33 ± 1.70	<0.0981

	C5-Sugar Alcohol	0.32 ± 0.25	0.51 ± 0.44	<0.2713	C5-Polyhydric Alcohol	0.76 ± 0.09	0.30 ± 0.15	<.0001
	Hexose/Ketose/Inositol	33.79 ± 0.89	28.83 ± 9.08	<0.1220	D-Galactosamine	0.20 ± 0.02	0.10 ± 0.04	<.0001
	Glucose/Fructose*	2.44 ± 0.50	6.63 ± 4.66	<0.0164	D-Raffinose	0.03 ± 0.00	0.00 ± 0.00	<.0001
	Glyceric Acid	0.25 ± 0.03	0.27 ± 0.09	<0.3792	D-Ribose	0.23 ± 0.02	0.23± 0.12	<0.9751
	Mannitol	0.99 ± 0.49	15.61 ± 21.54	<0.0587	E-1-O-Cinnamoyl-beta-D-Glucose	0.27 ± 0.01	0.91 ± 0.29	<.0001
	Methyl Beta-D-Galactoside	1.30 ± 0.08	1.40 ± 0.75	<0.7086	Erythritol	2.00 ± 0.57	2.27 ± 3.03	<0.8087
	-	-	-	-	Glycerol	0.62 ± 0.02	0.31 ± 0.23	<0.0017
	-	-	-	-	Hexose-6-Phosphate	0.19 ± 0.05	0.21 ± 0.27	<0.8405
	-	-	-	-	Hexose-Disaccharide	0.84 ± 0.13	0.24 ± 0.25	<.0001
Phospholipids	Lysophosphocholine181	0.01 ± 0.00	0.01 ± 0.03	<0.8247	-	-	-	-
	Lysophosphatidylethanolamine160	0.06 ± 0.02	0.13 ± 0.11	<0.0806	-	-	-	-
	Lysophosphatidylethanolamine181	0.03 ± 0.01	0.19 ± 0.25	<0.0788	-	-	-	-
Nucleic Acid	2'-Deoxyguanosine	0.03 ± 0.01	0.06 ± 0.05	<0.0568	3'Siderocalin	1.04 ± 0.09	0.46 ± 0.21	<.0001
	Adenine*	0.46 ± 0.23	1.14 ± 0.60	<0.0056	5-hydroxyindoleacetic acid	0.01 ± 0.00	0.00 ± 0.00	<.0001
	Cytidine	0.08 ± 0.05	0.19 ± 0.16	<0.0720	5-Methylcytosine Hydrochloride	0.03 ± 0.00	0.12 ± 0.08	<0.0066
	Guanine*	0.03 ± 0.03	0.51 ± 0.38	<0.0017	5,6-Dihydrouracil	0.07 ± 0.09	0.07 ± 0.05	<0.9373
	Guanosine	1.85 ± 0.88	2.50 ± 2.84	<0.5228	5'-Deoxyadenosine	0.18 ± 0.13	1.24 ± 1.74	<0.1060
	Hypoxanthine*	0.10 ± 0.08	1.60 ± 1.64	<0.0138	Allopurinol	0.48 ± 0.03	0.71 ± 0.37	<0.0908
	Inosine	1.11 ± 0.06	1.37 ± 0.73	<0.2982	Cytidine 2',3'-Cyclic Mono-Phosphate	0.07 ± 0.03	0.02 ± 0.04	<0.0250
	Thymine*	0.01 ± 0.01	0.12 ± 1.10	<0.0045	Cytidine	0.36 ± 0.27	0.67 ± 0.80	<0.3083
	Uracil*	0.18 ± 0.11	1.37 ± 1.20	<0.0090	Cytosine	0.09 ± 0.03	3.13 ± 2.68	<0.0060
	Urate	0.04 ± 0.01	0.15 ± 0.17	<0.0649	Iso-cytosine	0.33 ± 0.33	0.63 ± 0.75	<0.2989
	Uridine	0.60 ± 0.23	0.76 ± 0.87	<0.6067	N-Pai-Methyl-L-Histidine	0.17 ± 0.01	0.32 ± 0.11	<0.0021
	Xanthine*	0.18 ± 0.14	2.55 ± 2.57	<0.0140	Thiamine Monophosphate	0.06 ± 0.01	0.05 ± 0.03	<0.4377
	-	-	-	-	Thiamine	0.04 ± 0.01	0.03 ± 0.01	<0.3081
	-	-	-	-	Uracil	0.28 ± 0.19	1.66 ± 1.72	<0.0406
					Urate	0.04 ± 0.01	0.06 ± 0.05	<0.3744
					Uridine	0.09 ± 0.04	0.13 ± 0.14	<0.4839
Fatty Acid	6-Hydroxycaproic acid	1.60 ± 0.06	1.54 ± 0.39	<0.6620	Palmitoleic acid	0.01 ± 0.00	0.01 ± 0.00	<0.0004
	Linoleic Acid*	0.91 ± 0.36	11.22 ± 13.5	<0.0358	-	-	-	-
Flavonoids	4-Coumarate	0.13 ± 0.01	0.10 ± 0.07	<0.3274	4'-Hydroxy-5,6,7,8-tetramethoxy flavone	7.18 ± 0.48	0.48 ± 2.34	<.0001

DISCUSSION

Starch is a natural product of photosynthetic CO_2 fixation in green tissues. Formed by a-1,4 glucose linkages, starch exists in 2 forms, the soluble, small linear chain amylose and the highly branched insoluble amylopectin (Etxeberria *et al.*, 2007, 2009). High level of starch content in citrus leaves has been regularly used as a provisional indication of HLB presence in citrus trees. Once accumulated, starch in citrus leaves is not degraded (Goldschmidt *et al.*, 1996) even during the night cycles and remains in the leaves indefinitely.

Visual comparisons of leaf starch between leaves from HLB-affected and healthy (control) trees made with a 2% iodine solution present a clear contrast between these two perceived circumstances (Etxeberria *et al.*, 2007). However, although our initial observations of reflect an unmistakable accumulation of starch in HLB-affected trees (Achor *et al.*, 2010; Etxeberria *et al.*, 2007, 2009; Folimonova and Achor, 2010; Schneider, 1968), developmental and other biotic and abiotic factors also affect leaf starch content during the course of HLB/ citrus tree association, therefore adding a degree of uncertainty. Concurrently, qPCR, test for HLB has proven inconsistent at times as a result of several factors outlined by Gottwald (2010). The predictive ability of starch for HLB detection is higher in the HLB-infected leaves compared to healthy leaf samples. The observations of SEM indicated that disruption of phloem tissues might be the major contributor of disease symptoms of *C*Las infection in citrus cultivars and it was confirmed by q PCR later.

Citrus fibrous roots are vital for absorbing and transporting water, nutrients, and other endogenous plant growth regulators. The efficient functioning of these roots in Huanglongbing (HLB)-affected citrus trees is important for their survival. However, the scanning electron micrograph represents the dense fibrous root mass evident in healthy control trees. However, a significant loss in fibrous root mass was evident in all the HLB-affected trees a year after infection. Healthy trees also showed new root growth, whereas very little new root growth was observed in HLB-affected trees. Fibrous roots appeared black to dark brown in colour in diseased trees and light brown in healthy controls. These results also showed the phloem plugging in the xylem and phloem cells of *C*Las-infected citrus cultivars. In contrast, healthy citrus roots contained normal levels of starch granules inside the cells of the second order of roots of citrus. The Etxeberria *et al.* (2009) data supports the notion that the substantial changes in carbohydrate partitioning observed throughout the citrus tree may not only result from HLB infection but, in itself, cause the rapid decline and death of infected trees.

Kumar and Kiran (2018) also support our study of root analysis of infected citrus roots with healthy citrus roots. However, the degree of infection was again confirmed with the qPCR analysis. It had been reported that the LJ900 primer set produced an amplicon derived from the prophage repeats presented within the *C*Las genome while the reported range of Ct values for healthy samples is around 36.3 to 0 Ct detectable among the healthy in contrast to HLB-affected citrus samples (Morgan *et al.,* 2012). However, for the infected leaves, most copy number values were in the millions, with the highest being 4.50×10^6 (Ct=16.50), with the 3 exceptions in copy number, such as 1.39×10^3 (Ct=28.2) to 1.87×10^5 (Ct=21.1) while these values highlighted the HLB infection status designated as positive or negative (Morgan *et al.*, 2012; Roberts *et al.*, 2017). Mostly diseased leaves had been reported to show vein chlorosis from the midrib which was seen smaller in size. Studies conducted by numerous experts highlighted the symptoms of advanced, blotchy mottled, and twig dieback of citrus leaves which were close to the symptoms of mineral deficiencies (Gottwald *et al.*, 2012; Killiny *et al.,* 2017). While the Ct values correspond to hypothetical copy numbers of *C*Las amplicon from 0-139 which is marked as negative corresponding to the Ct value which was greater than the 30 Ct threshold reported for HLB infection status in citrus cultivars (Dala-Paula *et al.*, 2019).

Plant tolerance or susceptibility to vector-borne diseases varies depending on the nature of the plant pathogen or its associated vectors (Zahid *et al.,* 2023). Various physical structures (thorns, trichomes, leaf wax) are present in the plant body, establishing the plant's barrier defenses against herbivores and protecting the plant against vector-borne diseases. Various phytochemicals are generated within the plant, enhancing its defense mechanisms against pathogens and their hosts. Sometimes, plants that synthesize these antimicrobial compounds and allelochemicals become more tolerant to pathogens. Thus, the citrus cultivars with these defensive metabolites should include the more disease-tolerant cultivars, ultimately reducing the cost of insecticide usage and citrus production (Killiny *et al.,* 2018; Qamar *et al.,* 2023). Herein, we study the primary and secondary metabolites involved in the citrus greening disease.

Understanding these metabolomics profiles in citrus cultivars can help identify and annotate biological markers which can predict the ability of tolerance and susceptibility in citrus to *C*Las infection. Global metabolomics analysis (LC-MS) results are divided into main metabolites groups: organic acids, fatty acids, carboxylic acids, phenols and their derivatives, flavonoids, nucleic acids, and amino acids. The upregulation and downregulations of the primary and secondary metabolites were observed in citrus healthy and *C*Las-infected leaf samples.

Amino acids are plants' main source of energy, regulating the root and shoot architecture in stress defense mechanisms and flowering time (Hao *et al.,* 2016). Phloem sap of the HLB-affected citrus varieties showed distinct concentrations of ten different amino acids when compared to healthy. Amino acids with the highest absolute loading value in PLSDA were L-arginine, L-glutamine, L-isoleucine, L-serine, L-tyrosine, L-valine, L-glutamine, L-asparagine, L-methionine, L-tryptophan, 3, 4 dihydroxy-L-phenylalanine, oxoproline. Herein, the current study indicated the probability rate of $p \leq 0.05$ of L-phenylalanine, L-methionine, L-valine, L-serine, asparagine, L-tyrosine, and L-isoleucine in leaves. Many other studies also indicated that phenylalanine, asparagine, and tyrosine are involved in the defense action mechanism of citrus with regard to pathogenic infections (Balan *et al.,* 2018). The end product of the shikimate pathway was phenylalanine, which produces specific amino acids including tyrosine and tryptophan as an end product (Odhong *et al.,* 2019). These amino acids are also the precursors for the phenylpropanoid pathway and are also intricate in the plant's defense action (Vogt 2010) in response to biotic stress (Cevallos-Cevallos *et al.,* 2011). L-phenylalanine showed an increased level in *C*Las-infected leaves. It is the main precursor involved in the upregulation of genes involved in the defense mechanism against biotic stresses. It was involved in the salicylic acid pathways. Increased rates of phenylalanine are consistent with many other studies in different plants such as soya bean, cucumber, and melon. These results showed that phenylalanine was higher in rate in healthy when compared to infected leaves with a high probability rate ($p \geq 0.05$). The elevated level of phenylalanine improves the flavor of citrus fruit and various other fruits like tomatoes, grapes, mango, etc. (Rao *et al.,* 2018). In the infected samples, twelve long-chain fatty acids/carboxylic acids and their conjugates were profiled (ascorbic acid, 3-

hydroxy decanoic acid, glycolate, caffeate, nicotinamide, arachidonic acid, tartaric acid, fumaric acid, succinic acid, oxalosuccinic acid, linoleic acid, D-saccharic acid) which indicating that the degree of infection has different metabolomics effect on citrus leaves. Nucleic acids (guanine, cytidine, adenine, uracil, xanthine) and sugars (disaccharide, glucose, fructose, hexose, ketose, inositol, S-mannitol) were quantified and seen decreased in amount in the infected samples with the probability rate of $p \leq 0.05$.

Carbohydrates and organic compounds are considered the leading indicators of the quality of fruit (Tang *et al.,* 2018). Herein, the amount of glucose and fructose found decreased in *C*Las-infected leaves when compared to healthy leaves. Carbohydrates/sugars act as a transporter of photo assimilation in the citrus phloem. Carbohydrates travel with the resorption theory, in which they can travel from the source (mature leaves) to the sink (in the phloem of mature fruit) as a transporter of photo assimilation. These results were consistent with other studies which explained that the photo-assimilate translocators were impaired by *C*Las-infection status in citrus cultivars (Kim *et al,.* 2009). Sugars/Carbohydrates and their derivatives are the main constituents of the cell structure and work in the metabolomics pathways against infection. Moreover, carbohydrates act as signaling complexes that can alter gene expression in the development and growth of plants. Sugars induction and accompanying inhibitory responses associated with photosynthesis have been observed in many plants (Hijaz *et al.,* 2018). Additionally, Smeekens, and Fan et al. demonstrated the decreased concentration of sucrose, glucose, and fructose involved in photosynthesis, which accumulated the starch level in mature leaves (Smeekens, 2000; Fan *et al.,*2010). HLB-infected leaves showed decreased levels of sugars when compared to healthy ones which resulted in the severe degradation of chlorophyll. The major symptoms of Huanglongbing include accumulating starch content in the leaves and phloem impairment. The decrease in sugars during systemic infection could reflect altered carbohydrate transport.

Huanglongbing interferes with sugar and starch metabolism and hinders the transport of nutrients in the phloem of plants. Ethylene causes sugar accumulation in leaves and a reduction in flavonoid production in the fruit. Different types of coumarins, flavonoids, and lignins are also involved in the plant's phenylpropanoid pathway and

defense action (Fraser, 2011). In this study, six different types of flavonoids (eujambolin, 4-coumarate, ganglioside, 4-hydroxy-5,6,7,8-tetramethoxy flavone, hesperidin, neo hesperidin) showed the wider differences between healthy and *C*Las-infected leaves. Flavonoids act as an antioxidant in citrus plants. Increases in the concentration of polyphenolic compounds such as flavonoids (Eujambolin, 4-coumarate, 4-Hydroxy-5,6,7,8-Tetramethoxy Flavone, Naringin, Hesperidin, neohesperidin, and Vanniloside) were seen in *C*Las-infected leaves compared to healthy leaves. Some citrus flavonoids and their derivative are prominent for promoting citrus bitter taste in fruit. Higher levels of flavonoids such as hesperidin have been shown to modulate the harsh metallic taste flavor in citrus fruit (Paula *et al.,* 2017; Paula et al., 2018; Ortiz et al., 2022)

The higher levels of phenols and polyphenols in healthy citrus plants were observed in many studies (Safdar *et al.,* 2017). In this study, phenols (hydroquinone, pyridoxine, mevalolectone, monobutyl phthalate) and phenolic compounds were seen to increase in *C*Las-infected citrus leaves compared to healthy leaves. Phenolic compounds act as feeding deterrents for herbivores and possess significant antioxidant activities. They also work against fungi, bacteria, and nematodes. Higher phenolic compounds make citrus plants less attractive to herbivores and enhance resistance to biological stress and the deleterious effects of pathogenic attack. A positive correlation of phenolic compounds was observed in the leaves of citrus cultivars with *CLas infection*. Other studies have also observed the distinct levels of phenolic compounds in different fruits and vegetables (Soares *et al.,* 2017). There were six organic acids whose derivatives (glutarate, shikimic acid, pimelic acid, phosphocholine, glyoxylic acid, and xanthurenic acid) were profiled in this study with $p \leq 0.05$. Other important groups of metabolites such as carboxylic acids and fatty acids are also seen in this study. Reduced concentrations of D-saccharic acid, oxalosuccinic acid, citrate, succinate, 3-hydroxy decanoic acid, 4-oxoproline, citramalate, and palmitoleic acid were observed in *C*Las- infected leaves ($p \leq 0.05$). Reduced concentrations of fatty acids in *C*Las-infected citrus plants were also detected by Suh et al*.* (Suh *et al.,*2018).

These results also found significant differences ($p \leq 0.05$) in some organic acids in leaf samples of healthy compared to *C*Las- infected citrus cultivars, such as Glutarate, Glycolate, Gallic Acid, Xanthurenic acid, Gluconic acid, Glyceraldehyde/Lactate, Glyoxylic acid, Phosphocholine,

3-(4- HydroxyPhenyl) Lactate, Nicotinamide, and Monobutyl Phthalate. Other studies have also shown increased levels of organic acids in citrus cultivars (Hijaz *et al.,* 2018). Additionally, organic acids in many plants increase in response to biotic and abiotic stresses, which presumably provides a protective function (Killiny *et al.,* 2016). As with carbohydrates, nucleic acids decreased in infected leaf samples. Metabolic profiling is currently the primary approach that provides insights regarding changes in targeted and untargeted metabolites potentially associated with tolerance to Huanglongbing disease (Adeniji *et al.,* 2020). Taken together, with these metabolic profiling results we can improved the basic nutrients in citrus (Pandey et al., 2022) and improve the physiology and biochemistry of citrus fruit with improved defense responses in favor of growth. Tolerance may be attained by understanding the pathways which was regulated by these defensive signalling metabolites. For examples, carbohydrates are the main target for bacterial pathogens, and we can induce defense against *C*Las by altering modification in sugars in citrus (Pandey et al., 2022). We believe that the data generated in this global metabolomics study will provide important information about potential biomarkers for the early and later stages of *C*Las infection of citrus cultivars and lay the groundwork for future investigations. Overall, the present work will provide context for the study of disease mechanisms that could be helpful in citrus breeding and horticultural programs worldwide.

CONCLUSION

HLB have huge impact on the citrus world industry. It had been evidenced from the current study's findings that the strategy of HLB-infected cultivars may sustain plant growth and phloem formation, which aided the plant defense mechanism to overcome the disease by using these metabolites as molecular markers. The findings of a study which are reported in the present manuscript could be used as a base for a deep understanding of the mechanism involved in the transportation of both micro and macronutrient, especially in the case of phloem blockage. The present study's outcomes could also be used to understand better the pathogenicity process and fruitful and novel strategies to control the harmful impact of *C*Las infection in citrus. Further metabolomic studies could be used to figure out the detailed list of targeted and untargeted metabolites such as amino acids, carboxylic acids, fatty acids, nucleic acids, carbohydrates/sugars,

flavonoids, phospholipids, organic acids, and phenols for the ease of future researchers. This study provided a detailed understanding of insight into the metabolomic studies of various citrus (leaves) infected with huanglongbing. Global metabolomics insight may give more approach for future study in the plant defense mechanism related to citrus greening. Based on the current evidence regarding metabolomics profiling, major defensive compounds are an effective strategy for the induction of diseased tolerant varieties of citrus. In conclusion to overcome the HLB, these metabolites will be used as a molecular marker. Generally, high levels of volatile compounds and lesser the availability of certain carbohydrates with flavonoids make lesser the survival of *C*Las infection and fruit quality will be restored. In future metabolomics approaches helped in understanding the host defensive pathways which was hijacked by the *C*Las bacterium and alteration in host metabolomics machinery will leads to the resistant citrus varieties to HLB.

REFERENCES

Balan, B., A. M. Ibáñez, A. M. Dandekar, T. Caruso and F. Martinelli. 2018. Identifying host molecular features strongly linked with responses to huanglongbing disease in citrus leaves. Frontiers in plant science, 9: 277.

Brennan, L. 2017. The nutritional metabolomics crossroads: how to ensure success for dietary biomarkers. Oxford University Press. Place Published. pp.293-94.

Celis-Morales, C., C. F. Marsaux, K. M. Livingstone, S. Navas-Carretero, R. San-Cristobal, R. Fallaize, A. L. Macready, C. O'Donovan, C. Woolhead and H. Forster. 2017. Can genetic-based advice help you lose weight? Findings from the Food4Me European randomized controlled trial. The American Journal of Clinical Nutrition, 105: 1204-13.

Cevallos-Cevallos, J. M., R. García-Torres, E. Etxeberria and J. I. Reyes-De-Corcuera. 2011. GC-MS analysis of headspace and liquid extracts for metabolomic differentiation of citrus huanglongbing and zinc deficiency in leaves of 'Valencia'sweet orange from commercial groves. Phytochemical Analysis, 22: 236-46.

Clarke, C. J. and J. N. Haselden. 2008. Metabolic profiling as a tool for understanding mechanisms of toxicity. Toxicologic Pathology, 36: 140-47.

Dala-Paula, B. M., A. Plotto, J. Bai, J. A. Manthey, E. A. Baldwin, R. S. Ferrarezi and M. B. A. Gloria. 2019. Effect of huanglongbing or greening disease on orange juice quality, a review. Frontiers in plant science, 9: 1976.

Fan, J., C. Chen, R. Brlansky, F. Gmitter Jr and Z. G. Li. 2010. Changes in carbohydrate metabolism in Citrus sinensis infected with 'Candidatus Liberibacter asiaticus'. Plant Pathology, 59: 1037-43.

Fraser, C. M. and C. Chapple. 2011. The phenylpropanoid pathway in Arabidopsis. The Arabidopsis Book/American Society of Plant Biologists, 9.

Gottwald, T., J. Graham, M. Irey, T. McCollum and B. W. Wood. 2012. Inconsequential effect of nutritional treatments on huanglongbing control, fruit quality, bacterial titer and disease progress. Crop Protection, 36: 73-82.

Hao, G., E. Stover and G. Gupta. 2016. Overexpression of a modified plant thionin enhances disease resistance to citrus canker and huanglongbing (HLB). Frontiers in plant science, 7: 1078.

Hijaz, F., Y. Nehela and N. Killiny. 2018. Application of gamma-aminobutyric acid increased the level of phytohormones in Citrus sinensis. Planta, 248: 909-18.

Killiny, N. and Y. Nehela. 2017. Metabolomic response to Huanglongbing: Role of carboxylic compounds in Citrus sinensis response to 'Candidatus Liberibacter asiaticus' and its vector, Diaphorina citri. Molecular Plant-Microbe Interactions, 30: 666-78.

Kim, J. Sagaram US Burns JK Li JL Wang N. 2009 Response of sweet orange (Citrus sinensis) to 'Candidatus Liberibacter asiaticus' infection: Microscopy and microarray analyses. Phytopathology, 99: 50-57.

Morgan, J. K., L. Zhou, W. Li, R. G. Shatters, M. Keremane and Y.-P. Duan. 2012. Improved real-time PCR detection of 'Candidatus Liberibacter asiaticus' from citrus and psyllid hosts by targeting the intragenic tandem-repeats of its prophage genes. Molecular and Cellular Probes, 26: 90-98.

Odhong', C., A. Wilkes, S. van Dijk, M. Vorlaufer, S. Ndonga, B. Sing'ora and L. Kenyanito. 2019. Financing large-scale mitigation by smallholder farmers: what roles for public climate finance? Frontiers in Sustainable Food Systems, 3: 3.

Paula, B. M. D., S. Raithore, J. A. Manthey, E. A. Baldwin, J. Bai, W. Zhao, M. B. A. Glória and A. Plotto. 2018. Active taste compounds in juice from oranges symptomatic for Huanglongbing (HLB) citrus greening disease. LWT, 91: 518-25.

Qamar, M. A., M. Javed, S. Shahid, M. Shariq, M. M. Fadhali, S. K. Ali and M. S. Khan. 2023. Synthesis and applications of graphitic carbon nitride (g-C3N4) based membranes for wastewater treatment: A critical review. Heliyon: e12685.

Rao, M. J., F. Ding, N. Wang, X. Deng and Q. Xu. 2018. Metabolic mechanisms of host species against citrus Huanglongbing (Greening Disease). Critical Reviews in Plant Sciences, 37: 496-511.

Roberts, R., G. Cook, T. G. Grout, F. Khamis, I. Rwomushana, P. W. Nderitu, Z. Seguni, C. L. Materu, C. Steyn and G. Pietersen. 2017. Resolution of the identity of 'Candidatus Liberibacter'species from Huanglongbing-affected citrus in East Africa. Plant disease, 101: 1481-88.

Safdar, M. N., T. Kausar, S. Jabbar, A. Mumtaz, K. Ahad and A. A. Saddozai. 2017. Extraction and quantification of polyphenols from kinnow (Citrus reticulate L.) peel using ultrasound and maceration techniques. Journal of food and drug analysis, 25: 488-500.

Smeekens, S. 2000. Sugar-induced signal transduction in plants. Annual review of plant biology, 51: 49-81.

Soares, S., S. Kohl, S. Thalmann, N. Mateus, W. Meyerhof and V. De Freitas. 2013. Different phenolic compounds activate distinct human bitter taste receptors. Journal of agricultural and food chemistry, 61: 1525-33.

Suh, J. H., Y. S. Niu, Z. Wang, F. G. Gmitter Jr and Y. Wang. 2018. Metabolic analysis reveals altered long-chain fatty acid metabolism in the host by Huanglongbing disease. Journal of agricultural and food chemistry, 66: 1296-304.

Svatos, A. 2011. Single-cell metabolomics comes of age: new developments in mass spectrometry profiling and imaging. ACS Publications. Place Published.

Tang, N., N. Chen, N. Hu, W. Deng, Z. Chen and Z. Li. 2018. Comparative metabolomics and transcriptomic profiling reveal the mechanism of fruit quality deterioration and the resistance of citrus fruit against Penicillium digitatum. Postharvest Biology and Technology, 145: 61-73.

Zahid, A., Z. Mukhtar, M. A. Qamar, S. Shahid, S. K. Ali, M. Shariq, H. J. Alathlawi, M. A. Hasan, M. S. Khan and S. Islam. 2023. Synthesis of Mn-Doped ZnO Nanoparticles and Their Application in the Transesterification of Castor Oil. Catalysts, 13: 105.